Modelling influence of Poisson's contraction on squeeze film levitation of planar objects

A. Almurshedi ⓘ ; M. Atherton ⓘ ; C. Mares ⓘ ; T. Stolarski ⓘ

Check for updates

View Online

Export Citation

07 June 2024 16:25:33

AIP Publishing

Modelling influence of Poisson's contraction on squeeze film levitation of planar objects

View Online   Export Citation   CrossMark

A. Almurshedi, (iD) M. Atherton, (iD) C. Mares, (iD) and T. Stolarski (iD)

AFFILIATIONS

College of Engineering, Design and Physical Sciences, Brunel University London, Middlesex UB8 3PH, United Kingdom

ABSTRACT

Poisson's contraction effect is utilised to generate squeeze film levitation and is investigated through a computer model and validated experimentally. A finite element model (ANSYS) is verified by the experimental testing of five different plate designs. Each plate is subjected to uniaxial plain stress by an arrangement of two hard piezoelectric actuators bounded to the bottom of the plate and driven with DC and AC voltages. It is observed that a pulsating dimple or crest shape along the longitudinal axis in the central area of the plate is created due to Poisson's contraction, generating a squeeze-film between the plate and a levitated object. The separation distance between the floating planar object and the plate is analysed using computational fluid dynamics (ANSYS) and experimentally measured by a laser sensor. A good agreement has been found between model predictions and experimental results.

I. INTRODUCTION

A. Background

Frictionless or non-contact transportation is essential for manufacturing ultra-precision products in micro-fabrication and nanotechnology, for example, silicon wafers and integrated circuits, where tiny flaws, infinitesimal scratches, and contamination must be avoided. It is also indispensable for precision positioning and the manipulation of light planar objects.

Techniques such as air–bed flotation and magnetic levitation have been utilised practically for frictionless, non-contact production–line transportation. However, air–beds require a huge amount of clean air at high cost due to exterior equipment, e.g., piping and pumps, and magnetic levitation only works for ferrous material. Moreover, magnetic levitation cannot always be utilised for delicate objects due to strong magnetic flux. Consequently, there is considerable interest in developing new techniques for free suspension of delicate objects.[1–3]

The literature reveals that non-contact levitation, without using externally pressurised air, comprises three main approaches, namely, standing wave acoustic levitation (SWAL), near-field acoustic levitation (NFAL), and squeeze film levitation (SFL). However, the literature is often confused between these three approaches.[4–6] SWAL has a different working principle to NFAL; the former is only utilised for tiny particles, whereas the latter can be used for a heavier floating object. However, the principle underpinning both methods (SWAL and NFAL) is based on acoustic radiation pressure. In contrast, SFL

is fundamentally based on the Bernoulli principle and usually it is modelled using the Reynolds equation, requiring a closing gap in the direction of flow in order to create average pressure above ambient. The main parameter of a fluid flowing in the direction of a converging gap is its viscosity. Closing the gap is subsequently followed by its opening and the whole cycle resembles a pumping action. It should be noted that in some studies,[7,8] it is assumed that there is a similarity between NFAL and SFL, but in reality there are significant differences regarding their lifting force phenomena.

B. Poisson's contraction as a source of SFL

The overall aim of the paper is to demonstrate that Poisson's contraction effect created in a plate clamped at both ends and under the plane stress conditions can be the source of squeeze film levitation for light planar objects. Therefore, there is a potential to induce the SFL mechanism without operating the plate at resonant frequencies of vibration. Exciting an arrangement of piezoelectric actuators at many cycles per second produces periodic forces elongating a thin plate, which in turn results in a uniaxial plain state of stress and the formation of a dimple in the direction perpendicular to that of the applied uniaxial stress (Fig. 1).

Pulsating with controlled frequency, the dimple squeezes the air in the gap between the plate and the object, producing a sustained levitating force (Fig. 2). In other words, this is not a conventional vibrating plate where the vibration modes deform the plate
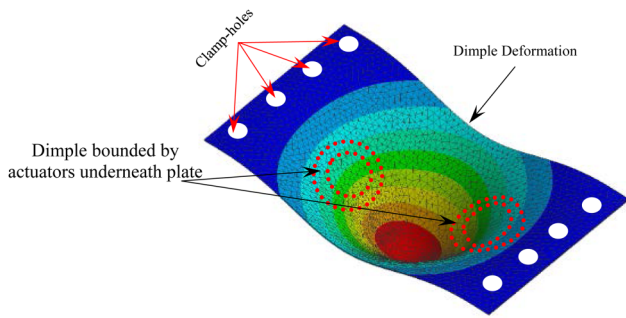
07 June 2024 16:25:33

FIG. 1. Finite element analysis simulation of plate dimple due to Poisson's ratio effect.

most at frequencies determined by plate geometry, material, and boundary characteristics. Therefore, the term "oscillation" rather than "vibration" is used here to avoid confusing oscillation of localised deformation due to Poisson's effect with that of modal shapes resulting from plate vibration.

II. THEORETICAL MODEL

A computer model of a system comprising of the plate together with a floating object is presented and executed using the finite element method (ANSYS Workbench).

A. Statement of the problem

The system modelled consists of a floating object and a flat thin plate with a single layer of hard piezoelectric actuators bonded

to the underside of the plate. The plate is firmly fixed at both ends, as shown in Fig. 3 and can be deformed repeatedly to create a dimple shape or a concave form in the downward direction at the centre of the plate. The deformation can be affected by many mechanical and electrical parameters. The most significant factor is Poisson's ratio coefficient of a material of the plate together with the supply voltage (DC: offset voltage; AC: amplitude voltage) to the piezoelectric actuators. The model presented in this paper is a simplified case of a centrally positioned pulsating dimple created by Poisson's effect. Undoubtedly, propagation of the initial deformation (dimple) as an elastic wave will establish a complex pattern of dimples all over the plate. This aspect of the problem is currently under further investigation by the authors.

B. Configuration of the plate

The geometry and main dimensions of the plate used for manufacturing are shown in Fig. 3. Various plate sizes and materials (Table I) have been theoretically and experimentally investigated. Two piezoelectric actuators (PZTs) are adequate for the design to produce a dimple shape of deformation. The actuators utilised were of rounded shape with 35 mm diameter and 0.8 mm thickness and were bonded to the underside of the plate.

C. Finite element modelling (FEM)

A simulation of the plate's deformation was carried out using the ANSYS Workbench transient structural analysis. Commands were written using a trigonometric equation (square wave equation), implemented with ANSYS mechanical APDL, and exported into ANSYS Workbench. The purpose of this was to actuate the PZTs with an On/Off time (Fig. 4) to make a central area of plate
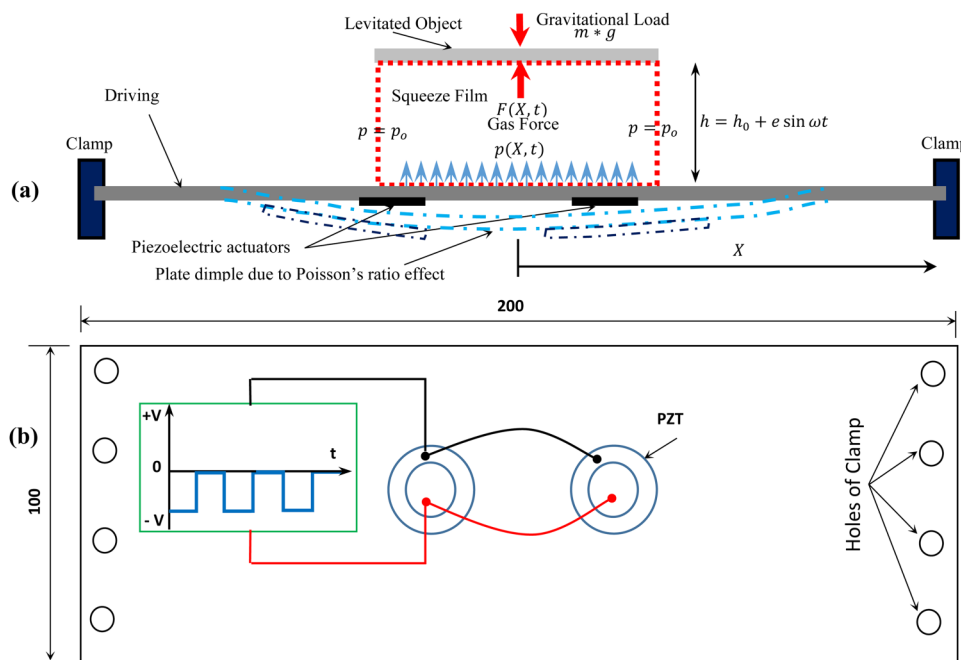

FIG. 2. (a) Side view of SFL generated by oscillating dimple due to Poisson's ratio effect. (b) Bottom view of the plate design and square wave voltage excitation; all dimensions in mm.
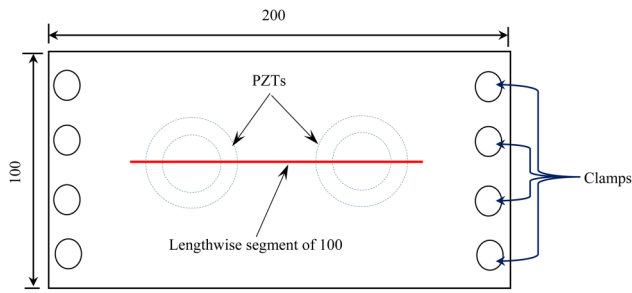
07 June 2024 16:25:33

FIG. 3. Top view of the plate design and lengthwise segment; all dimensions in mm.

deforming as a dimple in a downward direction as a concave form. The frequency excitation of the plate used in the ANSYS transient structural analysis simulation is the same as that used in the experimental test, which is 1.6 kHz.

In this study, static and dynamic (transient) analyses have been carried out for various plate designs. The purpose of the static analysis was to calculate the static deformation and to recognise the deformed shape of the plate designs when the piezoelectric actuators are operating with only a DC voltage. The aim of the dynamic analysis was to calculate the dynamic response of the plate by powering the piezoelectric actuators by an AC voltage. A square wave voltage signal (Fig. 4) has been used to drive the actuators. The purpose of driving the actuators by the square wave amplitude of voltage is to create distinct repeated contraction and elongation of the actuators. Consequently, the plate will respond generating a repetitive pocket or dimple shaped deformation in the downward direction at the central area of the plate.

The piezoelectric actuator has been modelled with a SOLID227 element, because this has 10 nodes with up to five degrees of freedom per node (UX, UY, UZ, VOLT, and TEMP—for definition of terms, see the Nomenclature). The structural capabilities include elasticity, plasticity, and large strain. It is a coupled-field element and is suitable for three dimensional (3D) analyses as well as being capable of modelling the piezoelectric actuator. The SOLID187 element was chosen to mesh the plate. It is a higher order 3D, with 10 nodes having three degrees of freedom at each node (translations in the nodal x, y, and z directions). Furthermore, piezoelectric elasticity stiffness and stress matrices have been included in the simulation throughout using the Piezo ACT (ANSYS Customization Toolkit) extension.

The finite element model (Fig. 5) and boundary conditions of the plate (Fig. 3) are presented and the material properties are listed (Table I). The plate has been modelled with three different materials: aluminium, stainless steel, and a polymer (polyethylene high density, HDPE). In addition, various sizes of plates have been simulated (Table I), where the effective length is 160 mm due to clamping at both ends. The boundary conditions applied are firmed boundaries on both ends of the plate and 150 V difference on each side of the actuators. The finite element mesh for one of the plate designs (Design A1) is shown in Fig. 5.

The piezoelectric elasticity stiffness matrix $[c]$ N/m^2, stress matrix $[e]$ C/m^2, and the relative permittivity matrix that have been utilised in the simulation are as follows:

$$[c] = 10^{10} * \begin{bmatrix} 13.2 & 7.3 & 7.1 & 0 & 0 & 0 \\ 7.3 & 11.5 & 7.3 & 0 & 0 & 0 \\ 7.1 & 7.3 & 13.2 & 0 & 0 & 0 \\ 0 & 0 & 0 & 2.6 & 0 & 0 \\ 0 & 0 & 0 & 0 & 2.6 & 0 \\ 0 & 0 & 0 & 0 & 0 & 2.6 \end{bmatrix},$$

$$[e] = \begin{bmatrix} 0 & -4.1 & 0 \\ 0 & 14.1 & 0 \\ 0 & -4.1 & 0 \\ 10.5 & 0 & 0 \\ 0 & 0 & 10.5 \\ 0 & 0 & 0 \end{bmatrix}.$$

The relative permittivity matrix is $\begin{bmatrix} 730 & 0 & 0 \\ 0 & 730 & 0 \\ 0 & 0 & 635 \end{bmatrix}$.

The PZT density is 7500 kg/m^3

D. Structural dynamics

The purpose of the dynamic analysis (transient) is to identify the dynamic characteristics of a structure exposed to dynamic driving loads. In this prototype design, the dynamic driving forces stem from the piezoelectric actuators when they are powered by an AC voltage. This is to produce enough displacement or to realise maximum dynamic reaction and thus achieve a better levitation.

TABLE I. Plates design configurations.

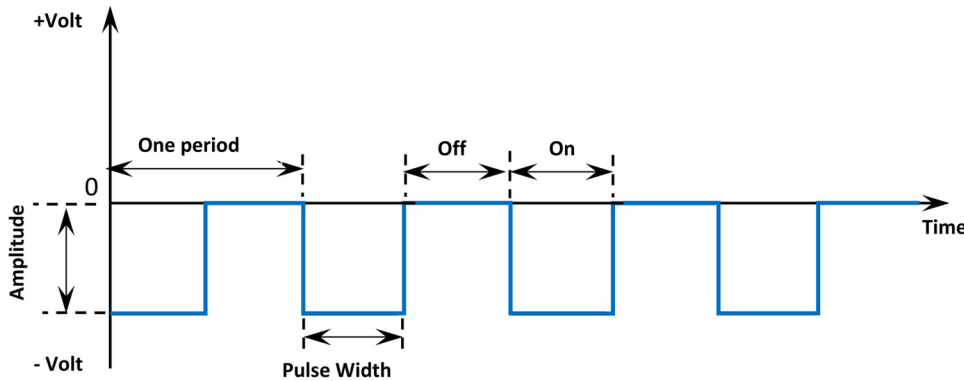| Design No.	Effective plate size, mm	Material	Modulus of elasticity, GPa	Density, kg/m^3	Poisson's ratio
A1	160*100*0.5	Aluminium	69	2676	0.33
A2	160*100*1				
A3	160*100*2				
B	160*100*0.5	Stainless steel	193	7781	0.33
C	160*100*2	Polyethylene high density (HDPE)	1.08	970	0.46

07 June 2024 16:25:33

FIG. 4. Square wave voltage signal to drive the PZTs.

1. Squeeze-film levitation modelling

An air film of certain thickness that is squeezed between the two surfaces with relative displacement of amplitude (e) at a frequency (ω), in the direction of the air film thickness, is assumed (Fig. 6). The pressure (p) at a point in the air-layer is controlled by the Reynolds equation.[7] So, the analysis of the squeeze-film dynamics is combined with the Reynolds equation which describes pressure within the air film and the equation of motion which governs the plate's movement.

The Reynolds equation can be expressed in general form[8,9] as specified by

$$\frac{\partial}{\partial x}\left(\frac{\rho_a h^3}{12\mu}\frac{\partial p}{\partial x}\right) + \frac{\partial}{\partial x}\left(\frac{\rho_a h^3}{12\mu}\frac{\partial p}{\partial y}\right)$$
$$= \frac{\partial}{\partial x}\left(\frac{\rho_a h (u_x + u'_x)}{2}\right) + \frac{\partial}{\partial y}\left(\frac{\rho_a h (u_y + u'_y)}{2}\right) + \frac{\partial (\rho_a h)}{\partial t}, \quad (1)$$

where ρ_a is the air density, h is the squeeze-film height, μ is the fluid viscosity, and t is the time. The time dependent term $\frac{\partial (\rho_a h)}{\partial t}$

is identified as the "squeeze term" as it signifies squeezing movement of the fluid. In addition, u_x, u_y and u'_x, u'_y refer to surface velocity components of bottom and top surfaces in the x and y directions, respectively.

Langlois[7] introduced a perturbation factor for pressure of the order of ϵ into the Reynolds equation and obtained the squeeze-film force which represents the one that develops because of the pressure variations (squeeze-film pressure and ambient pressure) for a given instant of time,

$$\frac{\partial}{\partial R}\left(RH^3 P \frac{\partial P}{\partial R}\right) = R\sigma \frac{\partial PH}{\partial T}. \quad (2)$$

The boundary conditions of squeeze-film for circular plates are assumed as

$$P(R, T = 0) = 1. \quad (3)$$

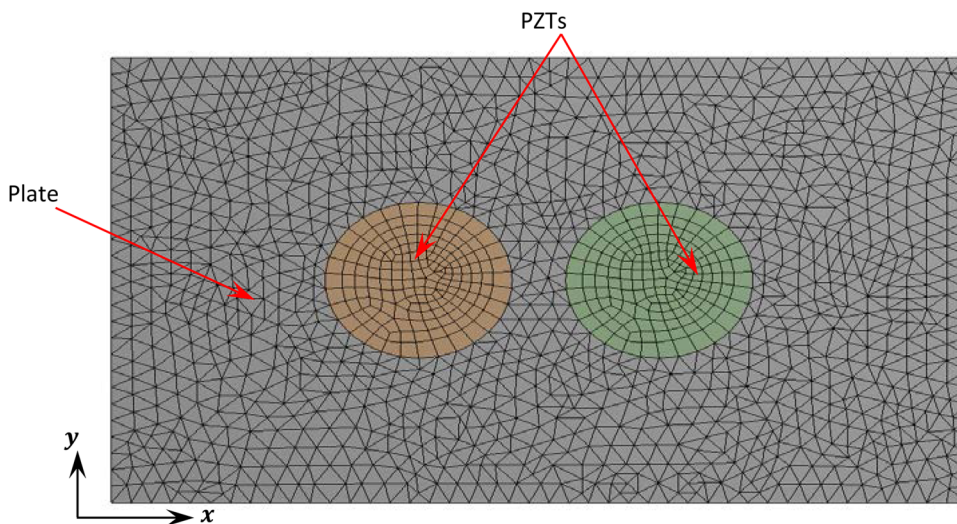The initial pressure between discs is atmospheric. At the outer periphery,

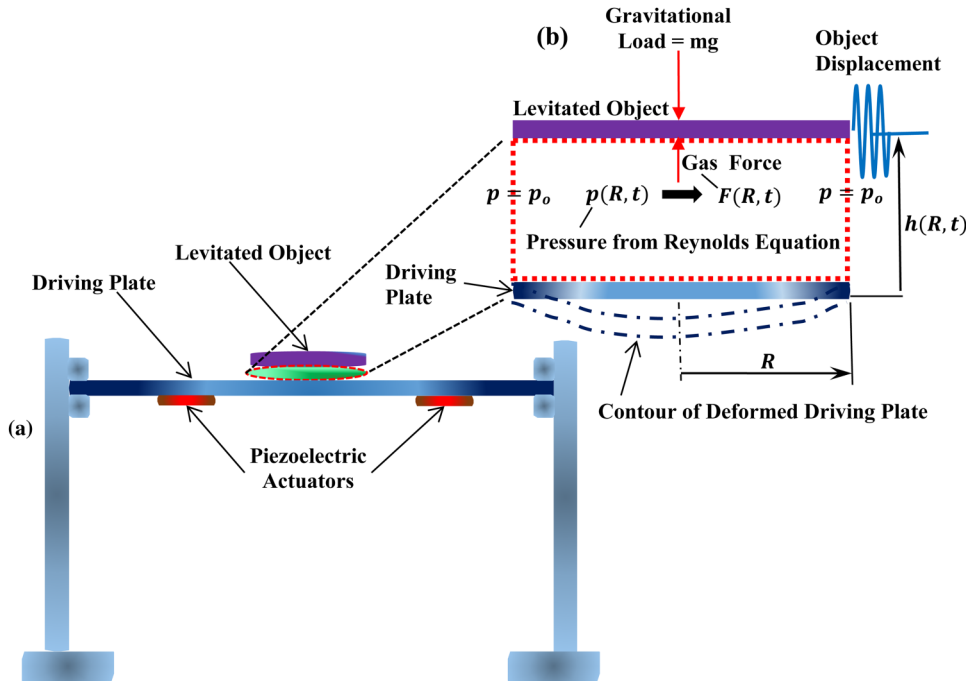**FIG. 5.** Mesh of a forced plate (Design A1), bottom view.

FIG. 6. Schematic design of the non-contact levitation: (a) Rig design; (b) Air film modelling (ANSYS—CFX).

$$P(R = 1, \ T) = 1, \tag{4}$$

$$\sigma = 12\mu R_0^2 \omega / p_0 h_0^2, \tag{5}$$

where σ is the squeeze number.

To explore the dynamic of squeeze-film approach, it is essential to take into consideration the coupled dynamics of the entire system (fluid and structural domains), which comprises the Reynolds equation and the equation of motion utilising a force equilibrium. Based on the free body diagram [Fig. 6(b)], the equation of motion can be expressed as

$$m\frac{d^2 z_t}{dt^2} = F_f - F_m, \tag{6}$$

$$F_f = \iint (p_j - p_0)rdrd\theta, \tag{7}$$

$$F_m = mg, \tag{8}$$

where F_f represents the fluid flow force which is evolved because of pressure variation and F_m is the weight of the floating object (circular plate) as employed in the simulation. The following expressions $z = h_0 Z$, $p = p_0 P$, and $\tau = t\omega$ can be used to make Eq. (7) dimensionless, where h_0 is the initial clearance, p_0 is an ambient pressure, and ω is the frequency of vibration,

$$\frac{d^2 Z}{d\tau^2} = \frac{p_0 r_0^2}{mh_0\omega^2} \iint (P_j - 1)RdRd\theta - \frac{mg}{mh_0\omega^2}, \tag{9}$$

$$z_t = z_l + h. \tag{10}$$

By differentiation of Eq. (10) with respect to time yields

$$\frac{d^2 z_t}{dt^2} = \frac{d^2 z_l}{dt^2} + \frac{d^2 h}{dt^2}. \tag{11}$$

The levitating height z_l in terms of motion source can be represented by $z_l = Z_0 \sin\tau$, thus

$$\frac{d^2 z_l}{dt^2} = -\omega^2 Z_0 \sin\tau. \tag{12}$$

Equation (12) can be rewritten in normalised form as

$$\frac{d^2 Z}{d\tau^2} = -\omega^2 Z_0 \sin\tau + \frac{d^2 H}{d\tau^2}. \tag{13}$$

Substituting Eq. (13) into Eq. (9) will produce the following expression:

$$-\omega^2 Z_0 \sin\tau + \frac{d^2 H}{d\tau^2} = \frac{p_0 r_0^2}{mh_0\omega^2} \iint (P_j - 1)RdRd\theta - \frac{mg}{mh_0\omega^2},$$

Or

$$\tag{14}$$

$$\frac{d^2 H}{d\tau^2} = \frac{p_0 r_0^2}{mh_0\omega^2} \iint (P_j - 1)RdRd\theta + \omega^2 Z_0 \sin\tau - \frac{mg}{mh_0\omega^2}.$$

Equation (14) is a second-order nonlinear partial differential equation and its initial conditions ($t = 0$) are given as $\frac{dH}{dT} = 0$ $P_n = 1$.

To understand the floating performance based on the behaviour of squeeze film, the equation of motion in addition to the Reynolds equation needs to be added and solved by means of numerical estimation.[10,11] The non-dimensional Reynolds equation can be modified into the dimensions (2D) though provided that the pressure is constant in the Y direction. Newton's Second Law can be applied to represent the equation of motion for the floating object.[11] Initially, the levitation force produced through the squeeze film action must be greater than the weight of the levitating object

for it to be levitated from rest, until equilibrium is reached at the maximum separation gap. The non-contact separation between the plate and the floating object can be inspected depending on the equation of motion coupled to the Reynolds equation with state boundary conditions.

2. Squeeze-film action

Squeeze-film levitation can be generated when an air-layer is entrapped between the two interacting surfaces. In fact, average pressure and resulting load carrying capacity that is produced by
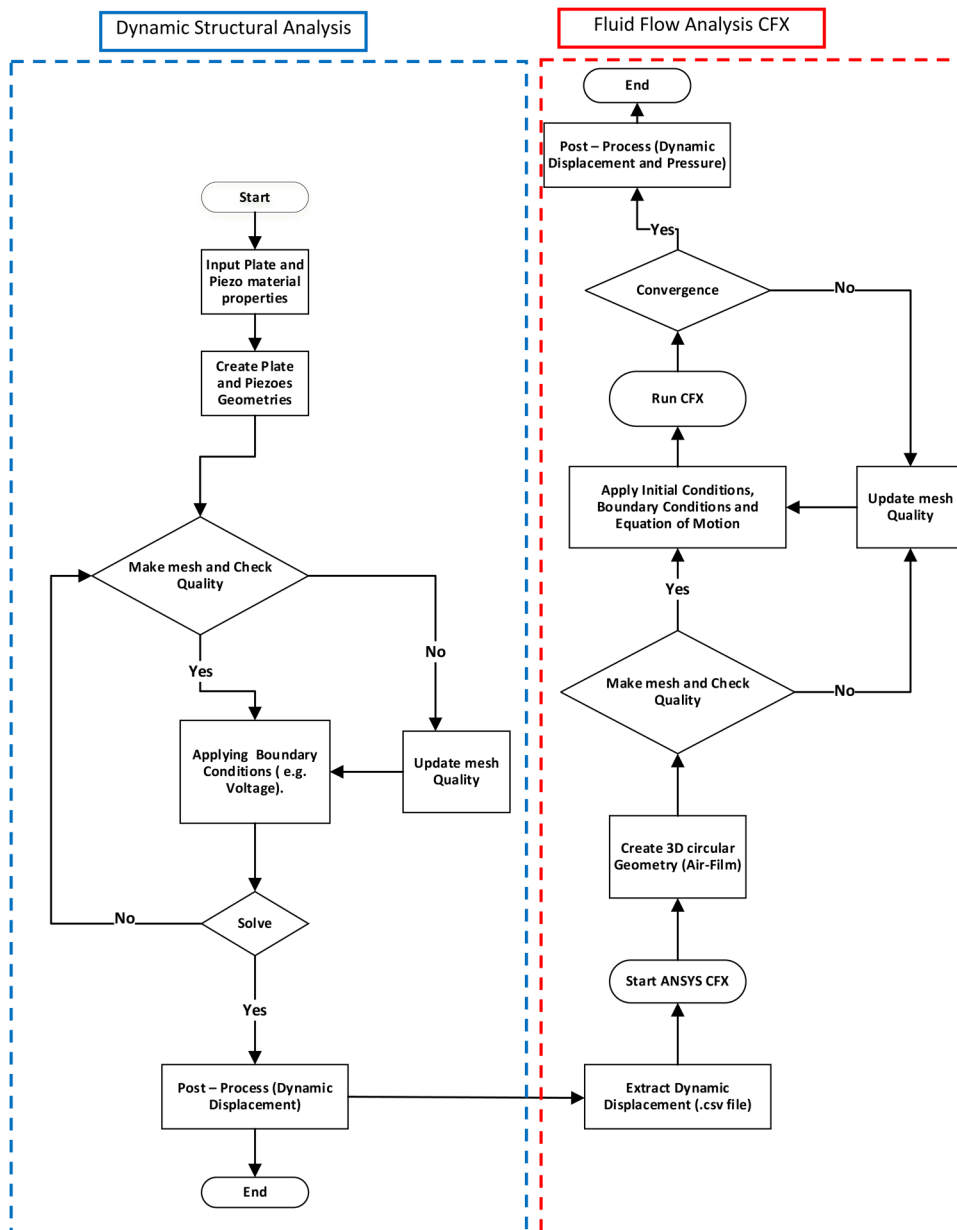

FIG. 7. Theoretical model flow chart.

the cyclic displacement at the layer produces complete support for a lightweight object [Fig. 6(a)].

When inertia and the tensional stresses in the fluid are negligible, the Reynolds equation is the main non-linear partial differential equation that defines the pressure distribution in the squeezed air film and can be evaluated through the Navier–Stokes and continuity equations. Furthermore, two important, instantaneous, and recurrent steps are behind the pressure distribution in the squeezed air film, which stem from the influence of the boundaries on the flow cycle. Hence, throughout the compression stage, the development in pressure forms an outward flow, while simultaneously the air layer between the surfaces reduces, letting only a slight airstream to occur. In contrast, during the decompression period, the pressure falls, and the stream alters to begin an inward flow. At this stage, the air-gap rises, letting a superior flow quantity pass in at a low velocity.[7]

E. Model of squeeze air-film in ANSYS CFX

A simulation utilising ANSYS CFD is implemented to examine the performance of a levitated object (freely suspended rigid mass). It is assumed that only one degree of freedom in the vertical direction is allowed. The instantaneous position of the object is evaluated by balancing its inertia, the fluid flow force made by pressure distribution and gravity. An air film that exists between a planar object (5 g disc) and a flat, rectangular plate (Fig. 6) of various designs is simulated. In other words, different case studies are implemented to identify the factors that affect the floating performance. The air film is of thickness 20 μm and it has the same area as the disc (35 mm, diameter) [Fig. 6(b)]. Three boundary conditions (named Top, Bottom, and Side) have been used to model the semi-cylindrical shape of the air-layer and to analyse the squeeze film levitation.

The top boundary condition refers to the bottom surface of the floating object and represents the mass of the floating object. The bottom boundary condition denotes the top surface of the plate design and indicates the bottom plane of the air film that has been modelled as a deformed boundary. It is given an amplitude (displacement) acquired from the plate that will squeeze the air film in the normal direction (Fig. 7). Finally, the side boundary condition has been modelled on the periphery of the air-layer as an open boundary, so the flow in this boundary is not restricted in any direction. In other words, the pressure value is identified (atmospheric pressure), but the direction of flow is unknown [Fig. 6(b)].

III. EXPERIMENTAL VALIDATION

A. Configuration of the apparatus

The schematic layout of the experimental work is shown in Fig. 8. The experimental apparatus comprises of an oscilloscope, DC power supply, AC power supply amplifier, signal generator, laser sensor, plate design rig, and piezoelectric actuators. The piezoelectric actuators of type PZT-4 are bonded to the bottom of the plate and are connected in parallel. The experiment requires the signal generator to create a certain signal voltage. The output terminal of the signal generator is connected to the amplifier of type ENP-1-1U (Echo Electronics) as it is essential to increase the voltage input from the signal generator. This produces a stable 15 magnification for the AC and DC signal inputs. Its operational point can be regulated to gain the appropriate bandwidth for the experimental measurements. The oscilloscope is used to read and display the output signals of the signal generator and the amplifier. The laser triangulation sensor from the Micro-Epsilon Company (type ILD-2300-5) is vertically placed above the plate design so as to achieve sufficiently accurate measurements according to the guide
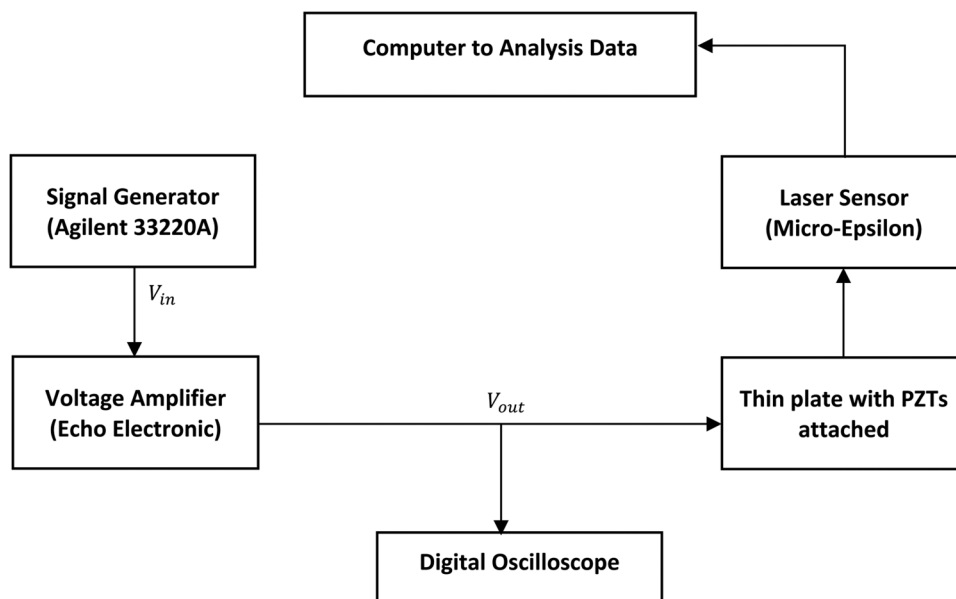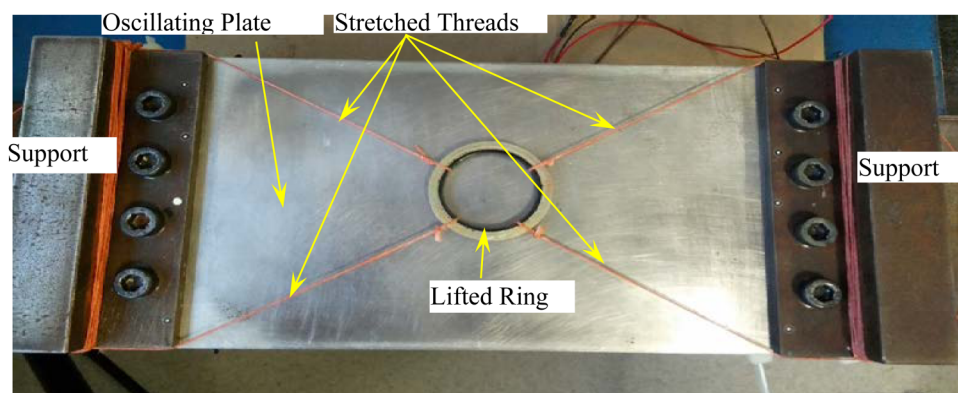

FIG. 8. Layout of the experimental work.

FIG. 9. Arrangement to constrain the sideway movement of a levitated object (disc).

setting provided by the company. The sensor captures the static and transient deformation of the plate design plus the levitation distance of the floating object (a disc of 5 g) without any contact. The output measurement data from the laser sensor are processed by special software provided by the Micro-Epsilon Company. For example, it can capture the entire output data without averaging, while having the ability to view the average estimated data. These measurements enable observation of the dynamic response of the plate designs and the floating object behaviour. Additionally, these measurements are used to validate the static and dynamic deformations calculated from the theory of the coupled-field analysis.

Moreover, in order to avoid sideways movement of the floating object and also to measure the normal separation, the disc is placed inside a suspended metal ring of inner diameter 5 mm larger than the disc diameter (Fig. 9). Four thin cords are stretched parallel to the ring and connected to a fixed support such that there is no contact between the ring and the plate design. In this way, the disc will only lift inside the ring in a normal direction (1-DOF) when the plate design is driven.

The PZTs offset the plate with an appropriate DC voltage (up to 150 V) and the plate is then dynamically excited by a square-wave AC voltage (Fig. 4) applied to the PZTs.

IV. RESULTS AND DISCUSSION

Simulations of one of the plate designs (Design A1), which show contour plots for the static (DC voltage) and transient (AC voltage) deformations, respectively, are shown in Figs. 10 and 11.

Static and transient deformations for a lengthwise segment (Figs. 12 and 13) in the central area of the top surface of the plate have been obtained using ANSYS Workbench and also measured experimentally for all five designs (Table I).

As can be seen from Figs. 10 and 11, the effect of Poisson's contraction is the formation of a dimple at the central area of the plate. This influence and the shape of deformation stem from the repeated expansions and contractions of the bounded piezoelectric actuators when they are operated by a square wave signal of voltage. The static results show that a high deformation of the plate occurs when high
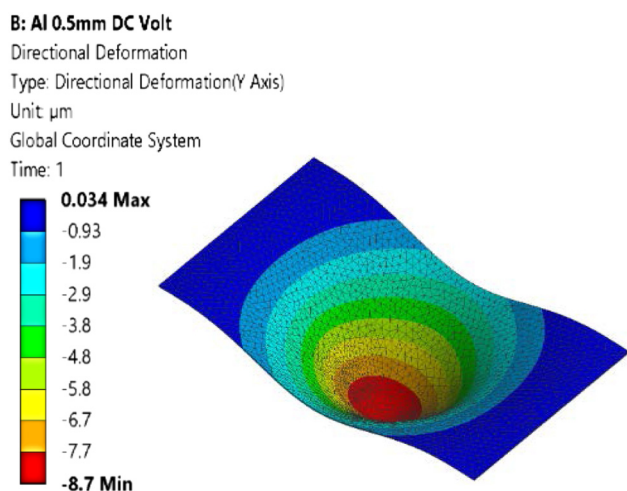
07 June 2024 16:25:33

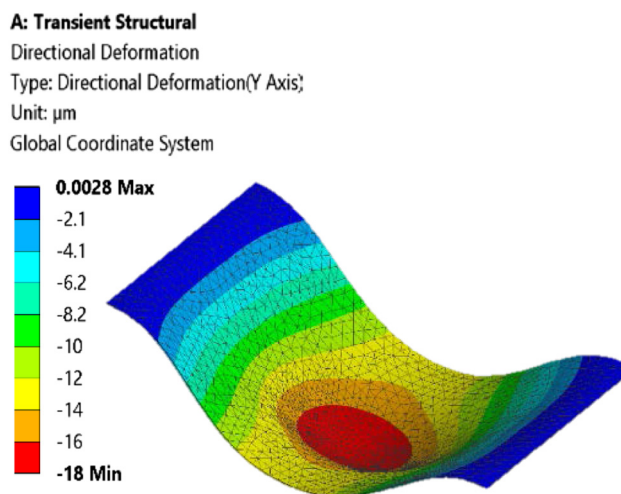

FIG. 10. Static (DC voltage) deformation (Design A1).

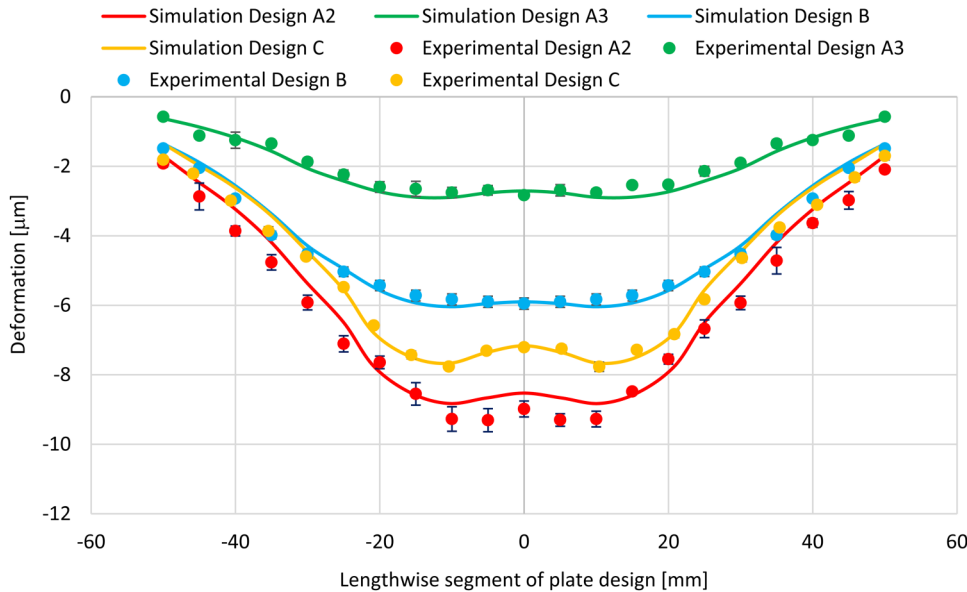FIG. 11. Transient maximum (AC + DC voltage) deformation (Design A1).

FIG. 12. Static (DC voltage) deformation, measurement, and numerical simulation for various designs, PZTs driven at 90 V DC.

voltages (90 V DC) are applied to the actuators and also with a thinner plate design[12,13] (Fig. 12). The plate Design A1 made of aluminium and of lesser thickness 0.5 mm delivers the highest deformation among the five plate designs (Fig. 12). If the operational voltage is in the linear domain of the piezoelectric actuator material, the deformations are directly proportional to the driving voltage. That is, the plate deformation increases as the applied voltage is raised.[14]

Furthermore, the variations in the experimental results for the plate deformation occurred because of many factors, such as the noise of electric devices (voltage amplifier and signal generator), the linearity of the laser sensor 1.5 μm, and the uncontrolled human movement inside and around the laboratory. The maximum deformation of the plate Design A2 [aluminium, of effective size (160 × 100 × 1 mm)] is of the order of 8.5 and 13.5 μm under the static and dynamic conditions, respectively (Figs. 12 and 13). Meanwhile, it has been estimated that the maximum deformation of the plate in the form of Design A3 [aluminium, of effective size (160 × 100 × 2 mm)] is of the order of 3 and 5 μm under the static and dynamic
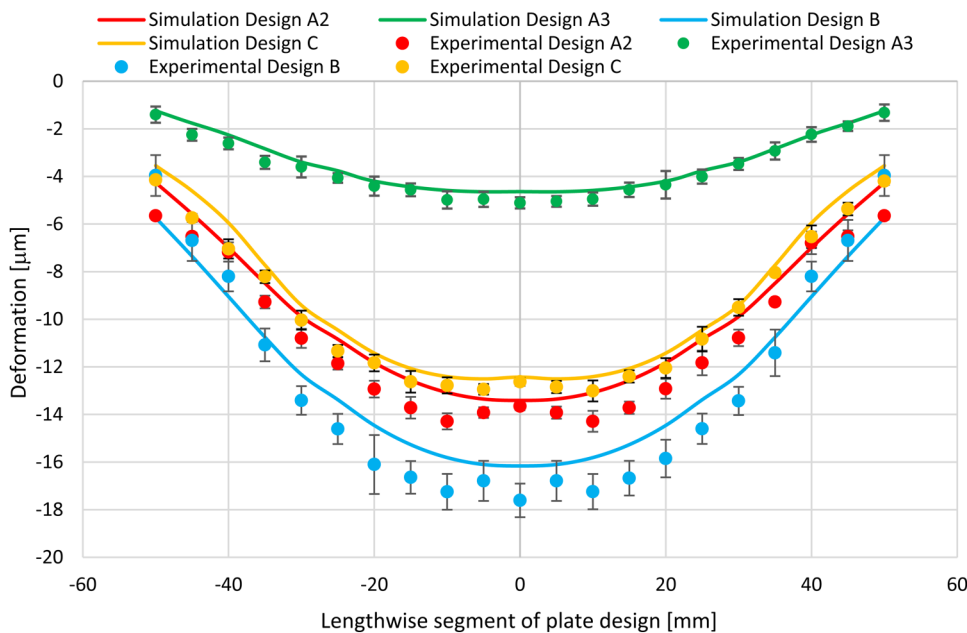

FIG. 13. Transient (AC + DC) deformation, measurement, and numerical simulation for various designs, PZTs driven at 150 V AC superimposed on 90 V DC.
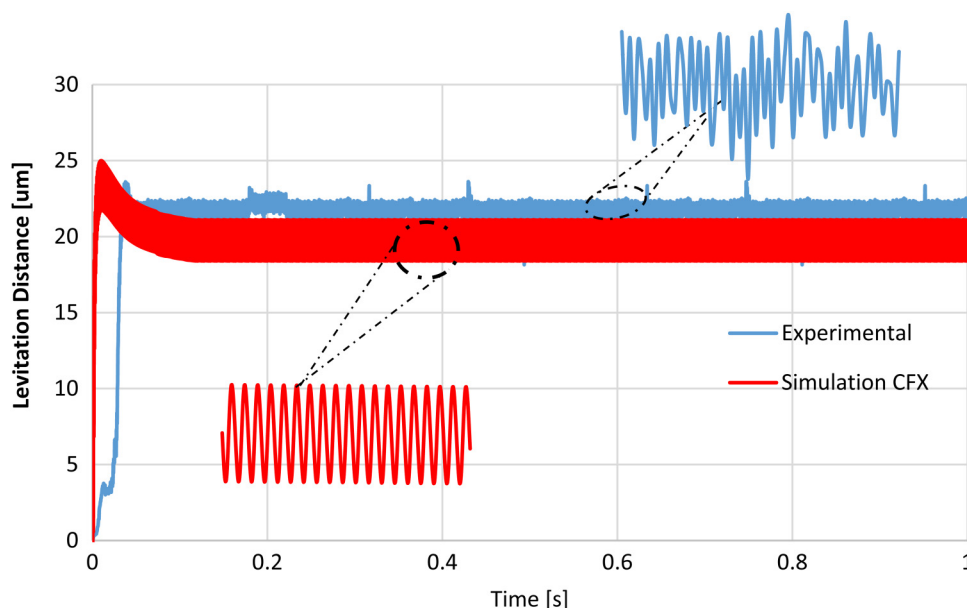
07 June 2024 16:25:33

FIG. 14. Levitation measurement and numerical simulation for Design A3, PZTs driven at 150 V AC superimposed on 90 V DC.

conditions, respectively. When this is compared to the maximum deformation of Design B (polyethylene, of effective size $160 \times 100 \times 2$ mm), which is of the order of 7 and 15 μm under the static and dynamic conditions, respectively, one must conclude that it performs better than Design A3 (Figs. 12 and 13). Hence, the contribution of Design B to the SFL can be considered as being significant. Furthermore, there is a good correlation between the experimental and simulation results of the deformation for all the plate designs.

The dynamic behaviour of the disc levitation for Design A3 (Fig. 14) has been investigated numerically utilising ANSYS CFD and measured physically using the Laser Sensor. The numerical simulation of dynamic levitation of the disc is achieved from when the time is equal zero and when the squeeze-film realises a pseudo-steady state (Fig. 14). A moving mesh technique has been employed to model the squeeze-film motion. The input parameters of levitation distance simulation
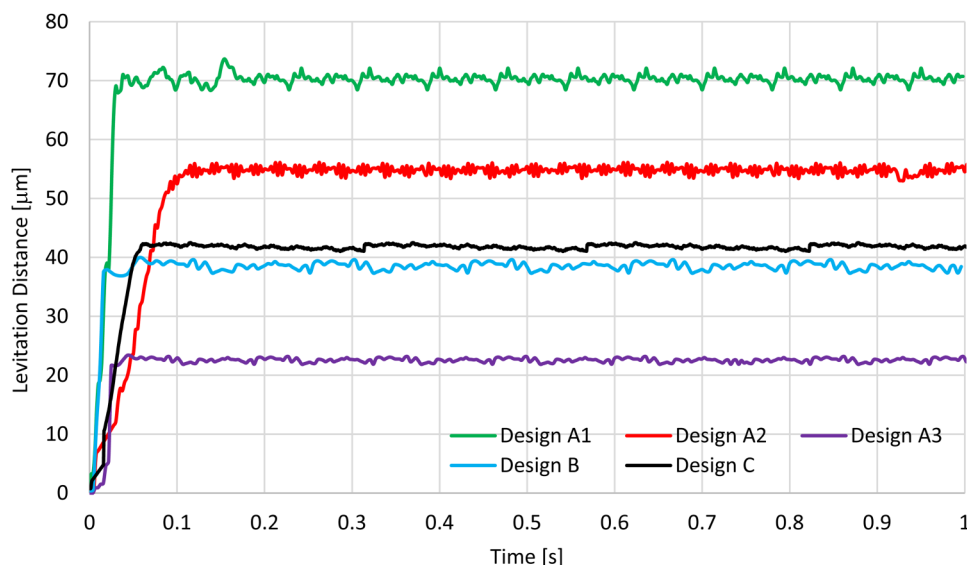

FIG. 15. Levitation measured for various designs, PZTs driven at 150 V AC superimposed on 90 V DC.

that have been utilised are film thickness at 20 μm, R = 35 mm, and load at the Top B.C of 5 g.

As can be seen from Fig. 14, one can observe that between times 0 and about 0.026 s, the surfaces (driving and floating) come in and out of mutual interaction. So, the surfaces can be in contact at the start-up, when the squeeze-film influence is not adequate to accomplish continuous normal separation of the floating object. The measured disc levitation with Design A3 (Fig. 14) is set to create an overshoot of separation of about 22.4 μm at a time of 0.0792 s, after which the separation tends to be at a steady state behaviour of about 21.1 μm. Meanwhile, the numerical simulation result of Design A3 (Fig. 14) has an overshoot of levitation of about 24.7 μm at 0.0001 s, and after about 0.0953 s, the dynamic levitation has established a complete squeeze-film action and tends to be at the steady state behaviour of about 20.8 μm, where it fluctuates at an average squeeze-film elevation (Fig. 14, enlarged display). Thus, the steady state error for both the experimental and theoretical results accounting for disc levitation obtained with Design A3 is about 1.44%.

The measurement results for Design A3 (Fig. 14) display some spikes due to the data being measured through the laser sensor entirely without averaging them. The levitation of the disc for the various designs has been illustrated as averaged results acquired through the laser sensor (Fig. 15). As can be seen, a steady state disc separation of 70 μm occurs with Design A1, which has a thinner plate. Design A2 creates a levitation for the same disc of about 54 μm, whereas a levitation of 22.3 μm occurs with Design A3, which has a thicker plate. Moreover, Design C shows a higher dynamic levitation of 41.85 μm than that produced by Design A3. In addition, Design B creates separation for the disc of 38.63 μm. It can be concluded from the results obtained for various plate designs that the disc separation is affected by the plate material more than the plate dimensions.

V. CONCLUDING REMARKS

Poisson's contraction effect on the squeeze film levitation has been investigated both theoretically and experimentally. The results of experimental measurements and simulation presented in this paper support the conclusion that the plate with PZT actuators driven by a conditioned signal voltage will create a cycling dimple deformation at the central area of the plate. Driving the PZT actuators with a square wave voltage signal is found to be effective for squeeze-film levitation, which has been confirmed both theoretically and experimentally for a planar object placed on the surface of the plate. Moreover, it has been observed that the plate design characteristics are additionally affected by a few other factors and, in particular, the plate size, material, and boundary conditions. The experimental measurements are consistent with the theoretical results for a one degree of freedom simulation. This could be further advanced by considering multiple degrees of freedom of the floating object.

NOMENCLATURE

c_a	Sound speed in air
F	Dimensionless bearing force/Radiation force
F_f	Fluid flow force (N)
F_m	Weight of the top surface (N)
g	Gravity (m/s^2)
H	Dimensionless film thickness
h	Film thickness (m)
h_0	Initial film thickness
k	Wave number
L	Length variable (m)
m	Mass of free floating item (kg)
P	Normalized pressure p/p$_0$ (Pa)
P_0	Ambient pressure
R	Dimensionless floating disc radius (m)
r_0	Radius of floating object (m)
T_a	Air temperature (K)
TEMP	Temperature degree of freedom
u_x, u_y, and u'_x, u'_y	Surface velocity components of bottom and top surfaces in x and y directions
UX	Displacements degree of freedom in the x axis
UY	Displacements degree of freedom in the y axis
UZ	Displacements degree of freedom in the z axis
V	Reference velocity (m/s)
VOLT	Voltage degree of freedom
X	Dimensionless form of x, X = x/L
Y	Dimensionless form of y
Z	Dimensionless floating disc displacement
Z_o	Initial displacement
z_l	Levitating height of disc (m)

Greek

ε	Dimensionless amplitude
μ	Dynamic viscosity (Pa s)
ν	Poisson's ratio
ω	Angular frequency (rad/s)
ρ_a	Air density (kg/m^3)
σ	Squeeze number $\sigma = (12 \mu \cdot \omega \cdot b^2)/(h_0^2 \cdot p_0)$
τ	Dimensionless time $T = \omega^* t$ (s)
ξ_0	Amplitude of oscillation

REFERENCES

[1]Y. Hashimoto, Y. Koike, and S. Ueha, "Transporting objects without contact using flexural traveling waves," J. Acoust. Soc. Am. **103**, 3230–3233 (1998).

[2]S. Ueha, Y. Hashimoto, and Y. Koike, "Non-contact transportation using near-field acoustic levitation," Ultrasonics **38**, 26–32 (2000).

[3]J. Hu, G. Li, H. L. W. Chan, and C. L. Choy, "A standing wave-type noncontact linear ultrasonic motor," IEEE Trans. Ultrason. Ferroelectr. Freq. Control **48**, 699–708 (2001).

[4]P. Liu, J. Li, H. Ding, and W. Cao, "Modeling and experimental study on near-field acoustic levitation by flexural mode," IEEE Trans. Ultrason. Ferroelectr. Freq. Control **56**, 2679–2685 (2009).

[5]W. Li, Y. Liu, and K. Feng, "Modelling and experimental study on the influence of surface grooves on near-field acoustic levitation," Tribol. Int. **116**, 138–146 (2017).

07 June 2024 16:25:33

[6]D. Ilssar, I. Bucher, and N. Cohen, "Structural optimization for one dimensional acoustic levitation devices—Numerical and experimental study," in *Proceedings of ISMA 2014—International Conference on Noise and Vibration Engineering, and USD 2014—International Conference on Uncertainty in Structural Dynamics* (2014), pp. 317–329.

[7]W. E. Langlois, "Isothermal squeeze films," Q. Appl. Math. **20**(2), 131–150 (1961).

[8]S. Yoshimoto, H. Kobayashi, and M. Miyatake, "Float characteristics of a squeeze-film air bearing for a linear motion guide using ultrasonic vibration," Tribol. Int. **40**, 503–511 (2007).

[9]B. J. Hamrock, S. R. Schmid, and O. J. Bo, *Fundamentals of Fluid Film Lubrication* (CRC Press, 2004).

[10]A. Minikes and I. Bucher, "Coupled dynamics of a squeeze-film levitated mass and a vibrating piezoelectric disc: Numerical analysis and experimental study," J. Sound Vib. **263**, 241–268 (2003).

[11]T. A. Stolarski and W. Chai, "Self-levitating sliding air contact," Int. J. Mech. Sci. **48**, 601–620 (2006).

[12]Y. Hashimoto, Y. Koike, and S. Ueha, "Near-field acoustic levitation of planar specimens using flexural vibration," J. Acoust. Soc. Am. **100**, 2057–2061 (1996).

[13]T. A. Stolarski and C. I. Woolliscroft, "Use of near-field acoustic levitation in experimental sliding contact," J. Appl. Mech. **74**, 816 (2007).

[14]R. Ghodssi and P. Lin, *MEMS Materials and Processes Handbook* (Springer Science & Business Media, 2011), Vol. 1.

07 June 2024 16:25:33